Communications Biology

https://doi.org/10.1038/s42003-026-09673-0

Article in Press

Salinity stress response of black yeasts isolated from deep-sea sediments of the Gulf of Mexico

Received: 2 July 2025

Accepted: 29 January 2026

Cite this article as: Camacho-López, M.D., Figueroa, M., Hernández-Melgar, A. *et al.* Salinity stress response of black yeasts isolated from deep-sea sediments of the Gulf of Mexico. *Commun Biol* (2026). https://doi.org/10.1038/s42003-026-09673-0

Maria Dolores Camacho-López, Mario Figueroa, Alan Hernández-Melgar & Meritxell Riquelme

Salinity stress response of black yeasts isolated from deep-sea sediments of the Gulf of Mexico

Maria Dolores Camacho-López[1]; Mario Figueroa[2]; Alan Hernández-Melgar[2]; Meritxell Riquelme[1]

[1]Department of Microbiology, Centro de Investigación Científica y de Educación Superior de Ensenada (CICESE), Baja California, Mexico.

[2] Facultad de Química, Universidad Nacional Autónoma de México, Ciudad de México, 04510, Mexico.

Correspondence

Meritxell Riquelme, Centro de Investigación Científica y de Educación Superior de Ensenada, Baja California, Mexico.

Email: riquelme@cicese.mx

Keywords: extreme halotolerance, yeast-like growth, endoconidiogenesis, melanin, metabolome.

Abbreviations: Gulf of Mexico, GoM; economic exclusive zone, EEZ; phthalide, PTH; 1,8-dihydroxynaphthalene, DHN.

Abstract

Fungi that live in deep-sea sediments experience extreme environmental conditions, yet little is known about how they adapt their growth and metabolism to these stresses. This study explores the morphogenetic and metabolomic responses of three black yeasts—*Salinomyces thailandicus*, *Neophaeotheca triangularis*, and *N. salicorniae*—isolated from deep-sea sediments of the Gulf of Mexico under varying salinities and exposure to the melanin inhibitor pthalide. Each species displays distinct growth adaptations: *S. thailandicus* shifts from filamentous to yeast-like forms as salinity increases, *N. triangularis* exhibits the opposite trend, and *N. salicorniae* remains dimorphic but grows more slowly at high salinities. Phthalide inhibits hyphal development in all three species. An exploratory metabolic analysis, conducted on pooled samples, indicates that metabolomic profiles change with salinity, with fatty acids dominating across species, suggesting membrane remodeling as an adaptation to osmotic stress. *N. triangularis* uniquely accumulates amino acids and peptides, a response previously reported mainly in plants. Additional metabolites, including aminocyclitols and compounds associated with extracellular polymeric substances, suggest the involvement of uncharacterized adaptive mechanisms contributing to stress protection. These findings advance our understanding of how black yeasts adapt to osmotic stress and provide a foundation for future studies.

Introduction

Despite the ecological and biotechnological importance of marine fungi, relatively few studies have explored their diversity in the Gulf of Mexico (GoM), a semi-enclosed sea and the world's ninth-largest body of water. Bordered by five U.S. and six Mexican states, the GoM was severely impacted by the 2010 Deepwater Horizon oil spill, which spurred research into its microbial life, including fungi[1-3]. Metagenomic studies have since revealed a high fungal diversity in deep-sea sediments within both the U.S. and Mexican exclusive economic zones (EEZ)[1,4], leading to the isolation of several filamentous fungi and yeasts, including black yeasts[2,5,6]. The diversity of black yeasts inhabiting saline environments remains poorly understood. Nonetheless, several known species have been isolated from halophytic plants, marine habitats, and hypersaline waters[7-9]

Black yeasts are a polyphyletic group of melanized fungi within the Ascomycota, encompassing species across the Arthoniomycetes, Dothideomycetes, and Eurotiomycetes[10]. Also referred to as meristematic or microcolonial fungi, black yeasts are characterized by pleomorphic growth, melanized cell walls, and the formation of daughter cells that are often embedded in a matrix of extracellular polymeric substances (EPS), which contribute to their resilience in extreme environments, such as hypersaline habitats[11].

Beyond their pleomorphic growth, black yeasts exhibit unconventional cell division patterns that differ from those of classic model yeasts, such as *Saccharomyces cerevisiae* and *Schizosaccharomyces pombe*, which divide by budding and fission, respectively, generating a single daughter cell per cycle. In contrast, black yeasts demonstrate environmentally responsive shifts in division modes, reflecting a high degree of morphological plasticity. Some species alternate between fission and budding, while others produce multiple buds simultaneously. Species such as *Neophaeoteca salicorniae* generate both yeast-like and filamentous cells, releasing dense clusters of progeny[7]. These division patterns can also vary with cell density[12]. Moreover, while it has been speculated that these unconventional division patterns are linked to the extreme environments these organisms inhabit, this hypothesis remains unsubstantiated.

The ability of black yeasts to persist under extreme conditions has made them the focus of increasing scientific interest[10]. For instance, *Hortaea werneckii,* capable of growing in media containing up to 30% NaCl, has emerged as a model organism for studying salt adaptation mechanisms[13]. Adaptation strategies employed by halotolerant fungi include the accumulation of compatible solutes, which help maintain osmotic balance and turgor without interfering with core metabolic functions[14]. Additionally, alterations in membrane lipid composition help preserve membrane fluidity, while melanin may accumulate on or within the cell wall to form a protective barrier against osmotic stress[15].

While melanin plays diverse roles in fungal biology, in black yeasts, it has been specifically implicated in osmoprotection by reinforcing the cell wall[16]. In many species, melanin, primarily synthesized via the 1,8-dihydroxynapthalene (DHN) pathway. This pigment is produced through the oxidative polymerization of phenolic or indolic compounds[17,18], and its biosynthesis can be selectively inhibited to investigate its function. Fungi produce three main types of melanin– DHN-melanin, pheomelanin, and pyomelanin – via different biosynthetic pathways that use distinct precursors, including DHN, levodopa (L-DOPA), and intermediates from tyrosine degradation[19]. These pathways can be selectively targeted; for example, kojic acid blocks pheomelanin synthesis without affecting the others[20].

Importantly, at the metabolomic level, the responses of halotolerant fungi to saline environments remain largely unexplored, with most studies focusing on filamentous fungi[21]. Given the capacity of black yeasts to survive across a wide salinity range, there is considerable interest in characterizing their metabolome. In addition to their adaptive physiology, halotolerant fungi are increasingly recognized as promising sources of novel secondary metabolites with potential applications in medicine, agriculture, and biotechnology[22]. Nevertheless, these fungi—particularly those from deep-sea environments—remain understudied.

In this study, we have investigated the black yeasts *Salinomyces thailandicus* (formerly *Hortaea thailandica*), *Neophaeotheca triangularis*, and *Neophaeotheca salicorniae* isolated from deep sediments of the GoM. We have examined their morphological and cellular responses to varying salinity concentrations and under melanin inhibition conditions and explored their corresponding metabolomic profiles to better understand the mechanisms of halotolerance and their potential for bioactive compound production.

Methods

Isolation and identification of black yeast species

Black yeast species were isolated from deep-sea sediments collected from the GoM (Mexican EEZ) at depths between 1,152 and 3,739 mbsl during the XIXIMI 7 campaign (May-June 2019) aboard B/O Justo Sierra, as part of the CIGoM (Gulf of Mexico Research Consortium) project (Fig. 1; Supplementary Table 1; Methodology Supplementary Information in Supplementary Material). These species are housed in the

Marine Fungi Collection of the Microbiology Laboratory at CICESE. Isolation sites are shown in Fig. 1., which presents a map generated using GeoMapApp (www.geomapapp.org) under a CC BY license.

Genomic DNA was extracted as previously described[23]. The internal transcribed spacer (ITS) region of nuclear ribosomal DNA (ITS1-5.8S rDNA-ITS2) and the D1/D2 domain of 26S rDNA were amplified using the universal primers ITS1F (5´-CTTGGTCATTTAGAGGAAGTAA-3´)[24], ITS4 (5´-TCCTCCGCTTATTGATATGC-3´)[25], NL1 (5´-GCATATCAATAAGCGGAGGAAAAG-3´), and NL4 (5´-GGTCCGTGTTTCAAGACGG-3´)[26]. PCR products were sequenced by Eton Bioscience, Inc. (San Diego, CA). Sequences were aligned using MEGA v12[27], and homologous sequences were identified by comparison with the GenBank database using BLAST[28]. Phylogenetic relationships were inferred using the Maximum Likelihood method under the Tamura-Nei (1993) model of nucleotide substitutions, and the tree with the highest log-likelihood value was selected[29].

Media and stress conditions

Czapek Dox modified medium was employed for all assays (2 g L^{-1} $NaNO_3$, 0.5 g L^{-1} $C_3H_7MgO_6P$, 0.5 g L^{-1} KCl, 0.35 g L^{-1} K_2SO_4, 0.01 g L^{-1} $FeSO_4$, 0.4 g L^{-1} glucose, pH 6.8±2)[30]. Halotolerance was tested across different NaCl concentrations (0-30%, increasing salinity by 5%). Selected concentrations of 0%, 3.5% sea salt, 10%, and 20% NaCl were used for growth, morphology, and cell division assays. Based on our observations of colony morphology in these species, where no changes were detected in medium without salt compared to 3.5% sea salt, but morphological alterations were observed at 10% and 20% NaCl (Fig. 2), we selected 0% and 10% NaCl to analyze, at the ultrastructural level, cells with and without PHT, as well as changes in the metabolomic profile under these same conditions. Malt extract agar (MEA) was used for culture maintenance at 23°C with constant light.

Growth, morphology, and cell division assays

Colonial morphology was analyzed on Czapek Dox solid media (60 mm diameter Petri dishes) inoculated with 10^5 cells and incubated for 15 days at 23°C ± 2. Cell division was assessed on Lab-Tek® Chambered #1.0 Borosilicate Coverglass Systems, inoculated with 5 x 10^4 cells in 600 µL Czapek Dox liquid medium, followed by a 24 h incubation period at 23°C ± 2 and 72 h filming. Growth was measured in triplicate on 96-well microplates with 10^5 cells and 190 µL of Czapek Dox liquid medium, incubated at 23°C ± 2 under 175 rpm shaking for 15 days. Optical density (OD_{600}) [31] was monitored every 24 h using a Multiskan Sky spectrophotometer (Thermo Scientific) with SkanIt RE software ver. 6.0.1.6.

Melanin inhibitors

Phthalide (PTH; P3960S, Sigma-Aldrich) and Kojic acid (K3125, Sigma-Aldrich) were used as DHN and DOPA-melanin inhibitors, respectively, at concentrations of 0.5, 1.0, 2.0, and 3.0 mg mL^{-1}. Based on the minimum concentration of PHT required to inhibit melanin production in each species, as observed in previous experiments, a concentration of 1.0 or 1.5 mg mL^{-1} was selected for further analyses of colonial and cellular morphology in Czapek medium supplemented with different salt concentrations: 0%, 3.5% sea salt, 10%, and 20% NaCl.

Optical Microscopy

Colonial morphology was documented using an Olympus IX81 stereoscopic microscope and an iPhone (13 Pro) camera. Cell morphology was examined using the inverted block technique [32] and an Olympus IX81 Cell Sens microscope (Apo N 60x/1.49 NA oil immersion objective). Cell division was observed using a Nikon ECLIPSE Ti microscope equipped with a HAMAMATSU C11440 ORCA-FLASH 4.0 camera, employing Differential Interference Contrast (DIC), Apo TIRF 60x/1.49 NA oil immersion objective, and ND Acquisition tool (autofocus) for automated 72 h time-lapse videos (with 10-min intervals between captures). Videos were acquired with NIS-Elements AR 5.30.03 and analyzed using Fiji[31,33] . All imaging was carried out at the CICESE National Laboratory for Advanced Microscopy.

Scanning and transmission electron microscopy

For scanning electron microscopy (SEM) and transmission electron microscopy (TEM), analyses were conducted using Czapek liquid medium formulated with or without 10% NaCl and supplemented with PHT at 1.0 mg mL^{-1} for *Neophaeotheca* and 1.5 mg mL^{-1} for *Salinomyces*. In each case, 9 mL of medium and 1 mL of pre-inoculum (OD_{600nm} = 2.0) were added to a 250 mL flask, and cultures were incubated for 6 days at 100 rpm and 23°C. Cells were collected by centrifugation at 1,400 x *g* for 5 min at room temperature. Samples were prepared for SEM and TEM as previously described[34] with some modifications. Briefly, the collected cells were fixed for 2 h in a 2.5% (v/v) glutaraldehyde solution prepared in phosphate buffer (pH 7.4), washed for 2 h in phosphate buffer (pH 7.4), and further fixed with 1% OsO_4 for 2 h. Dehydration was carried out using a graded ethanol series -20°C (25%, 50%, 75%, 90%, and 95%), with each step lasting 10 min, followed by two immersions in 100% acetone for 30 min each. For SEM, 20 µL of the fixed cells were placed on a microscope slide and covered with hexamethyldisilazane reagent. For TEM, cells were embedded in a series of 15%, 30%, 35%, 50%, 75%, and 100% of low viscosity Spurr Resin (PELCO® 18300-4221) that was polymerized in a mold at 60°C for 24 h. Samples were sectioned at 50-60 nm thickness with

a Leica ultramicrotome. Samples were analyzed using a Hitachi SU3500 SEM and a Hitachi H-7500 TEM at the CICESE National Laboratory of Advanced Microscopy.

Quantitative analysis of cell wall thickness was performed using micrographs processed with Fiji software. For each individual cell, the average of four measurements was recorded (*S. thailandicus*, n = 36; *N. triangularis*, n = 20; *N. salicorniae*, n = 28). A one-way ANOVA was employed to determine statistically significant differences among treatments.

Growth conditions and extract preparation

Cultures were grown in 250 mL liquid media, with and without 10% NaCl, and supplemented with either 1.0 mg mL^{-1} PTH for *Neophaeotheca* or 1.5 mg mL^{-1} PTH for *Salinomyces* species. Incubation was carried out under continuous light at 25°C with constant shaking at 110 rpm for 21 days. Control cultures lacked microbial inoculum. Given the slow growth and limited biomass production typical of black yeasts, and the exploratory nature of our study, extracts from two independent cultures were pooled to obtain sufficient material for metabolomic analysis. Cellular metabolism was halted by the addition of 10% MeOH. To separate the biomass from the liquid medium, samples were centrifuged at 8,000 × *g* for 30 min at 25°C using a Beckman Coulter Avanti JXN-26 centrifuge with a JA-14 rotor, and the supernatant was filtered through Whatman No. 1 filter paper. Metabolites from the biomass were obtained using a biphasic extraction with 50 mL of $CHCl_3$-MeOH (1:1) and MeOH-H_2O (1:1) solvent systems. Metabolites from the culture medium were extracted with 20 g L^{-1} of XAD16N resin (Amberlite® CAS-9003-69-4) and subsequently eluted with MeOH (see supplementary information for details). All extracts were concentrated to dryness using a rotary evaporator set at 40°C and stored at 4°C until use.

Analysis of extracts by UPLC-HRMS-MS/MS

Extracts (1 mg/mL in dioxane-MeOH 1:1) were analyzed using ultra-performance liquid chromatography (UPLC) coupled with high-resolution mass spectrometry in tandem (HRMS-MS/MS). An Acquity UPLC system (Waters Corp., Milford, MA, USA) and a Q Exactive Plus mass spectrometer (Thermo Fisher Scientific, Waltham, MA, USA) equipped with a heated electrospray ionization (HESI) source were used. Samples were separated on an Acquity BEH C18 column (50 mm × 2.1 mm I.D., 1.7 µm, 130 Å; Waters Corp.) at 40°C, with a gradient of 15-100 % CH_3CN in 0.1% aqueous formic acid over 8 min, followed by a 1.5 min hold at 100% CH_3CN, with a flow rate of 0.3 mL min^{-1} and an injection volume of 3.0 µL. The MS-MS/MS data were obtained in positive and negative modes (*m/z* 150-2000) with a top5 ions fragmentation

program, with the following parameters: capillary voltage of 5 V, capillary temperature of 300°C, tube lens offset of 35 V, spray voltage of 3.80 kV, and sheath and auxiliary gas flow at 30 arbitrary units.

Metabolomic analysis

MS/MS raw data were converted to .mzML format using the MS Converter tool from ProteoWizard and imported into MZmine 3.9[35]. The files were exported to the GNPS (Global Natural Products Social Molecular Networking) and SIRIUS platforms[36,37]. Based on previous studies[38], automatic metabolite annotation or identification at the structural level of the MS2 containing features using GNPS[39] was performed. The annotation of compounds, according to the Metabolomics Standards Initiative (MSI), was at a confidence level 2, based on the exact mass accuracy <5 ppm[40] and at level 3, based on the *in silico* tools MolDiscovery[41], CSI/FingerID[42], and DEREPLICATOR[43]. We retrieved the chemical classes of the features per group using the CANOPUS tool integrated with the SIRIUS software version 6.0.4[37,44]. Detailed information can be found in the supplementary materials.

Statistical analysis

GraphPad Prism version 9 was used to perform all graphs and statistical analyses presented in this article. One-way ANOVA and Tukey's multiple comparisons test were used to analyze the data (Details are provided in the Supplementary Data 1).

Data availability

Data sets of eukaryotic nuclear rRNA/ITS gene amplicon sequences were deposited in GenBank (database accession numbers shown in Table 1). LC-MS/MS data can be accessed at MassIVE (accession no. MSV000098170; accessed June 12, 2025), https://massive.ucsd.edu/ProteoSAFe/dataset.jsp?task=e9bb27d863a44851af057b411b5bd4e5. The parameters for feature-based molecular networking and spectral matching using all data sets, MolDiscovery, and DEREPLICATOR+ results are available in the links found in the Supplementary material.

Results

Black yeasts isolated from deep-sea sediments of the Gulf of Mexico exhibit halotolerance

Among the diverse fungal communities inhabiting deep sediments of the GoM, we successfully isolated three species of black yeasts. The strains P2_F1_L1, D1_F4_L1, and D9_S3_L1 were isolated from deep-sea sediment samples collected at sites E33, C23, and TS1 within the Mexican EEZ (Fig. 1). These sites correspond to the Tamaulipas-Veracruz continental slope, the Abyssal plain, and the Campeche saline canyon, at depths of 3,435, 3,739, and 2,417 mbsl, respectively. Molecular identification based on ITS and D1/D2 rDNA sequence analysis revealed that the isolates correspond to *Salinomyces thailandicus* (P2_F1_L1), *Neophaeotheca triangularis* (D1_F4_L1), and *Neophaeotheca salicorniae* (D9_S3_L1) (Table 1). Phylogenetic analysis supported these identifications, with strains P2_F1_L1 and D1_F4_L1 exhibiting high sequence homology and clustering with the respective type strains of *S. thailandicus* and *N. triangularis*. Although strain D9_S3_L1 displayed a higher percentage of sequence identity to the type strain of *Nothophaeotheca mirabibensis* (CBS 146980^{T}; NG_076740) than to the type strain of *N. salicorniae* (CBS 141299^{T}; NG_058237), phylogenetic analyses clearly placed these taxa in distinct clades. Notably, D9_S3_L1 clustered more closely with the *N. salicorniae* isolate CON1B8 (MN309703.1) (Supplementary Fig. 1).

Given that these species were isolated from a marine environment with a salinity of approximately 3.5%, we assessed their capacity for halotolerance by culturing them in media containing NaCl concentrations ranging from 0% to 30%. Colonies began to appear after seven days and were monitored for growth for up to 90 days to allow full development. All three species exhibited robust growth across a wide salinity range (0% to 20% NaCl, with the exception of *N. salicorniae*, which exhibited negligible growth at 20% NaCl) (Fig. 2), indicating salt tolerance plasticity. According to the definition of extreme halotolerance—growth at NaCl concentrations exceeding 15% (w/v)[45] — all three species are classified as extremely halotolerant fungi.

Black yeasts exhibit morphological plasticity in response to salinity

Due to the remarkable halotolerance, we investigated whether the three isolated black yeast species modify their morphology, growth, and cell division in response to salinity variations. For all experiments, the same culture medium was used, varying only the salt concentration, ensuring that observed cellular changes were solely due to salinity. *S. thailandicus* exhibited filamentous growth and formed rough, elevated colonies in media without salt and with 3.5% sea salt. In hypersaline conditions, it adopted a yeast-like morphology, forming colonies with an irregular shape, undulated edges, a viscous surface, and

convex elevation (Fig. 3A). In contrast, *N. triangularis* displayed the opposite trend: yeast-like growth and similar colony characteristics (irregular shape, undulated edges, mucoid surface) in low-salinity media (0%-3.5%), and filamentous growth with raised, viscous colonies under hypersaline conditions (Fig. 3B). *N. salicorniae* showed both yeast-like and filamentous growth under all salinities tested. However, filamentous and punctiform colonies were more prominent at 3.5% sea salt and 10% NaCl, with a viscous surface and pulvinate elevation, compared to the 0% and 20% NaCl conditions (Fig. 3C).

Growth rate of the black yeasts is salinity-dependent

All three species exhibited optimal growth at 3.5% sea salt, consistent with their marine origin. *S. thailandicus* grew best at 3.5% sea salt and in the absence of salt, with growth declining significantly as salinity increased (10%–20% NaCl) (Fig. 3D). *N. triangularis* grew well at 0%-3.5% sea salt and 10% NaCl, with a sharp decrease at 20% NaCl (Fig. 3E). *N. salicorniae* exhibited the lowest overall growth (note differing Y-axis scales) but grew best at 3.5% sea salt and 10% NaCl, and significantly less at 20% NaCl (Fig. 3F).

Salinity influenced cell division and morphogenesis

We monitored cell division for 72 h via time-lapse imaging. In *S. thailandicus,* yeast-like cells (aseptate or with 1-2 septa) underwent unilateral or bilateral budding, meristematic growth, and filamentation, contributing to microcolony formation (Fig. 4A-B). Time to budding was salt-dependent; unilateral budding was slower in 0% salt (10.1 h ± 2.1; n=12) compared to 10% NaCl (7.2 h ± 1.2; n=21), and 3.5% sea salt (8.3 h ± 1.0; n=26) (Fig. 4C; supplementary movie 1). Bilateral budding was also slower in 0% salt (11.8 h ± 3.9; n=39) compared to 3.5% sea salt (6.9 h ± 1.0; n=17) and 10% NaCl (7.9 h ± 1.2; n=16). No budding occurred at 20% NaCl (Fig. 4C; supplementary movie 1). Cells undergoing bilateral budding were larger (7.7 µm ± 1.0 x 3.2 µm ± 0.3) than those with unilateral budding (5.2 µm ± 1.0 x 2.5 µm ± 0.3), and cell size decreased with increasing salinity (Table 2). During cell division, daughter cells remained close to or attached to the mother cell and released melanin and other substances, likely EPS, which appeared to promote microcolony stability (Supplementary movie 1).

A comparable endoconidiation process was observed in *N. triangularis* and *N. salicorniae*. In both species, aseptate endoconidia developed a primary septum, followed by orthogonal septation, leading to the formation of muriform cells. These cells subsequently swelled, and endoconidia were released through the rupture of the mother cell wall (Figs. 4D, 4G). Notably, *N. triangularis* exhibited filamentous growth at

salinities above 3.5%, with endoconidiation initiating in distal regions and progressing toward the apex (Fig. 4D f-g, 4E; supplementary movie 2). At lower salinities, it retained a yeast-like morphology (Fig. 4D a-e, 4E; supplementary movie 2). In contrast, *N. salicorniae* formed filaments in salt-free medium (Supplementary movie 3) but adopted yeast-like growth at salinities above 3.5% (Fig. 4H; Supplementary movie 3). Time-lapse imaging revealed that cell division was salt-dependent. In *N. triangularis*, aseptate cells required 53 h (0% salt; n=3), 35 h (3.5% sea salt; n=4), and 44 h (10% NaCl; n=4) to divide and release endoconidia. Septate cells divided in 43 h (0% salt; n=4) and 32 h (3.5% sea salt, n=4), while muriform cells completed division in 30 h (0% salt, n=7) and 29 h (3.5% sea salt; n=7) (Fig. 4F). Cells displaying polarized growth in 10% NaCl medium divided and released endoconidia at the distal zone withing 40 h. No division was observed at 20% NaCl (Supplemental video S2). For *N. salicorniae*, muriform cells formed and released endoconidia within 29 h at 3.5% sea salt (n=4) and 42 h at 10% NaCl (n=4). No division occurred at 0% or 20% NaCl during the 72 h observation period (Supplementary movie S3). Cell size also responded to salinity. In *N. triangularis*, cells were larger at 0% and 20% NaCl than at 3.5% sea salt and 10% NaCl. Aseptate cells measured 5.0-5.6 µm, septate cells 6.6-8.7 µm, and muriform cells 9.3-11.2 µm (Table 2). In contrast, *N. salicorniae* showed consistent cell sizes across all salt concentrations, averaging 5.1 µm for aseptate cells, 7.0 µm for septate cells, and 9.0 µm for muriform cells (Table 2).

***S. thailandicus*, *N. triangularis,* and *N. salicorniae* use the DNH-melanin synthesis pathway**

Melanin production in black yeasts is recognized as an adaptation response to salinity stress[46]. While the DHN-melanin synthesis pathway has been previously identified in *N. triangularis* and other black fungi, its presence in *S. thailandicus* and *N. salicorniae* had not been confirmed. To investigate this, we used PTH and kojic acid, known inhibitors of the DHN- and DOPA-melanin synthesis pathways, respectively[47]. All three species showed reduced pigmentation when treated with PTH: at 1.5 mg mL^{-1} for *S. thailandicus* and 1.0 mg mL^{-1} for *N. triangularis* and *N. salicorniae* (Fig. 5A, arrows; Supplementary Fig. 2). In contrast, dark pigmentation remained unaffected under treatment with kojic acid (Fig. 5A), indicating that DOPA-melanin synthesis is not involved. These results confirm that *S. thailandicus*, *N. triangularis*, and *N. salicorniae* produce melanin via the DHN-melanin pathway (1,8-dihydroxynaphthalene melanin) (Supplementary Fig. 2).

Melanin has a role in filamentous growth

All three black yeast species eventually exhibited filamentous growth across all tested salt concentrations, except for *N. triangularis*, which displayed filamentous growth only at salt concentrations above 3.5% (data

not shown). Inhibition of DHN-melanin synthesis by the addition of PHT resulted in an almost complete suppression of filamentous growth. Under these conditions, only yeast-like cells were observed in both *S. thailandicus* and *Neophaeotheca* species (Fig. 5B).

Effect of melanin inhibitor on cell wall thickness

Halotolerant and halophilic fungi often employ osmoadaptive strategies, such as the production of glycerol and other osmolytes, to maintain osmotic balance and cellular turgor. In black yeasts, melanin accumulates in the cell wall, and it has been hypothesized that it reduces the permeability of glycerol, the smallest and most abundant polyol in *H. werneckii*[46]. To explore whether similar mechanisms are present in *S. thailandicus*, *N. triangularis*, and *N. salicorniae*, we cultured these species with and without 10% NaCl and with and without PTH and used TEM to examine ultrastructural changes in the cell wall under these stress conditions.

In *S. thailandicus*, a continuous layer of melanin granules was observed within the cell wall. This layer was noticeably thicker and denser in cells grown in salt-free medium than in those cultured with 10% NaCl (Fig. 6). Under PHT treatment, the melanin layer was thinner in salt-free conditions, whereas in 10% NaCl, melanin granules formed a distinct layer. Melanin was consistently detected on the outer surface of the cell wall in all conditions (Fig. 6A). Cell wall thickness varied significantly between salt-free medium (440 nm) and medium supplemented with 10% NaCl (570 nm) without PHT. Conversely, in the presence of PHT, cells exhibited thicker walls in the salt-free condition (866 nm) and a significant reduction in thickness under 10% NaCl (649 nm) (Fig. 6C).

In *N. triangularis*, small melanin granules accumulated on the outer layer of the cell wall under all tested conditions, except in 10% NaCl without PTH, where a discontinuous layer of larger melanin granules was observed. Extracellular melanin release was also evident (Fig. 6A). Cell wall thickness did not differ significantly between the salt-free medium (345 nm) and the medium containing 10% NaCl (325 nm). However, the addition of PHT led to a marked increase in cell wall thickness in the salt-free medium (460 nm), which was significantly greater than both the PHT-treated 10% NaCl condition (315 nm) and the untreated salt-free condition (Fig. 6C).

In *N. salicorniae*, melanin appeared as a discontinuous layer within the cell wall, accompanied by extracellular deposits, across all salt and PTH conditions (Fig. 6A). Cell wall thickness did not vary significantly, ranging from 293 nm to 343 nm across treatments (Fig. 6C).

Close-up imaging in all three species revealed the accumulation of additional translucent molecules within the cell wall, with some even traversing it to reach the extracellular space (Fig. 6B). This pattern of melanin and other molecule deposition was consistently observed across all examined cells.

Both SEM and TEM images revealed melanin granules traversing the cell wall and being deposited extracellularly (Fig. 7). Remarkably, in *Neophaeotheca* species, channels or pores traversing the cell wall were observed, often containing melanin granules that likely originated in the cytoplasm and migrated through these structures to the extracellular space (Fig. 7). In *N. triangularis*, the average channel thickness was smaller in salt-free medium (74.7 ± 8.6 nm without PHT; 85.7 ± 17.7 nm with PHT) compared to 10% NaCl medium (92.2 ± 18.6 nm without PHT; 135.5 ± 46.2 nm with PHT). In *N. salicorniae*, the channel thickness was smallest in 10% NaCl without PHT (79.7 ± 12.5 nm) and larger under all other conditions: salt-free without PHT (152.3 ± 78.3 nm), salt-free with PHT (166.6 ± 86.1 nm), and 10% NaCl with PHT (133.4 ± 59.7 nm). Channels were not evident in *S. thailandicus*.

Metabolomic profiling of black yeasts under salt stress and melanin inhibition

Across all growth conditions, and within an exploratory framework, a total of 355 features in ESI+ mode and 148 features in ESI– mode, were detected and annotated to the chemical class or structural level with a ≤ 5 ppm error, with a few exceptions corresponding to features previously reported in other fungi, for which we provide evidence of their detection in these black yeast species (Supplementary Data 2). The dominant metabolic classes included fatty acids, terpenoids, amino acids/peptides, carbohydrates, and alkaloids. In contrast, shikimates/phenylpropanoids and polyketides were rarely detected (Fig. 8A). Figure 8B and Supplementary Data 2 summarize metabolites detected in both biomass and culture supernatant extracts and their occurrence across experimental conditions at the superclass level, based on CANOPUS classification within NPClassifier. The largest number of metabolites was detected in the biomass extracts of all three species. Only a few fatty acids, alkaloids, tripeptides, and nucleosides were identified in both the biomass and supernatant, or exclusively in the supernatant. *N. triangularis* grown in a salt-free medium was the only strain in which 13 metabolites were detected in the biomass extract, 13 in the supernatant, and 9 in both fractions (Supplementary Data 2).

A comparative analysis of metabolic profiles between salt-free and 10% NaCl culture conditions revealed interspecific differences (Table 3). Only fatty acids and terpenoids were consistently detected under both saline conditions, whereas the presence of other metabolic classes varied depending on the salinity. Notably, at the intraspecific level, the putative metabolites identified under salt-free conditions differed from those detected under 10% NaCl, except for the octadecanoid 9,12,13-trihydroxyoctadec-10-enoic

acid (*m/z* 329.2328 $[M-H]^-$), detected under both conditions in *N. triangularis*, and the fatty acid (10*E*)-13-hydroxy-14-pentyl-1-oxacyclotetradec-10-en-2-one (*m/z* 297.2424 $[M+H]^+$), found under both conditions in *N. salicorniae*. In contrast, the *N*-acyl amine *N*-(carboxymethyl)-*N*,*N*-dimethyl-3-(tetradecanoylamino)propan-1-aminium (*m/z* 371.3273 $[M]^+$), was exclusively detected under salt-free conditions in all three species. Conversely, the octadecanoid 18-hydroxyoctadeca-9,12-dienoic acid (*m/z* 297.2424 $[M+H]^+$) was only detected under 10% NaCl in *S. thailandicus* and *N. salicorniae*.

Individually, *S. thailandicus* showed a reduced production of fatty acids and amino acids/peptides, an increased production of terpenoids and alkaloids, and no detectable production of carbohydrates or shikimates/phenylpropanoids under 10% NaCl conditions compared to the salt-free medium. In *N. triangularis*, cultivation under 10% NaCl led to a notable increase in the diversity of amino acids/peptides and terpenoids, a reduction in fatty acid subclasses, and a complete absence of polyketides compared to the salt-free condition. Finally, in *N. salicorniae*, metabolite production was markedly restricted under high salinity, with only fatty acids and terpenoids detected in 10% NaCl medium. By contrast, cultures grown without salt produced more diverse metabolomes.

Remarkably, PHT treatment induced more pronounced changes in the metabolic profiles of the three black yeast species. Among these, an increase in carbohydrate-related features was observed in all species, especially under 10% NaCl. The number of features detected in *N. triangularis* tripled compared to the untreated condition. Moreover, *N. triangularis* exhibited a substantial increase in fatty acid-associated features under high salinity, including dicarboxylic acids, hydroxy-, epoxy-, and oxo-fatty acids, octadecanoids, as well as thromboxanes and prostaglandins (eicosanoids absent under PHT-free conditions). *N. triangularis* under PHT treatment, produced linoleic acid, 9(10)-EpOME, 6-keto-prostaglandin F1α and thromboxanes. In contrast, *S. thailandicus* and *N. salicorniae* synthesized various derivatives of oleic, linoleic, and stearic acids, including 9,10-epoxy-oleic acid, 13-keto-9Z,11E-octadecadienoic acid, and 8-hydroxy-9,10-epoxystearic acid (Supplementary Data 2). Finally, in *N. salicorniae* under 10% NaCl resulted in a broader diversity of features across different metabolic pathways, and *S. thailandicus* exhibited a complete absence of metabolites associated with amino acid and peptide biosynthetic pathways.

Regarding carbohydrate metabolism, PHT treatment resulted in increased production of disaccharides across all three species, along with the presence of several monosaccharides and purine nucleosides. Interestingly, the disaccharide 2-[2-[(3,4-dihydroxy-6,8-dioxabicyclo[3.2.1]octan-2-yl)oxy]-3,5-dihydroxy-6-(hydroxymethyl)oxan-4-yl]oxy-6-methyloxane-3,4,5-triol (*m/z* 493.1527 $[M+H]^+$) was consistently

detected in all three species under 10% NaCl and PHT treatment. Finally, PHT treatment also led to an increase in both the number and diversity of alkaloid and terpenoid features, particularly in *Neophaeotheca* species, where purine- and pyridine-derived alkaloids were detected under both saline conditions.

Terpenoid metabolism also exhibited marked changes under PHT treatment, particularly in *N. triangularis*, which, under both saline conditions (0% and 10% NaCl), consistently produced ergostane-type steroids, germacrane sesquiterpenoids, and cembrane diterpenoids. In the absence of salt, additional terpenoid classes were detected, including apocarotenoids and cyclofarnesane-type sesquiterpenoids. Conversely, under 10% NaCl, a notably wider range of terpenoid subclasses was observed, such as acyclic monoterpenoids; bisabolane-, eremophilane-, and caryophyllane-type sesquiterpenoids; dammarane- and protostane-type triterpenoids; labdane-, norlabdane-, norpimarane-, and norisopimarane-type diterpenoids; as well as cholane and cholestane steroids, triketide meroterpenoids, and ecdysteroids.

In contrast, *N. salicorniae* displayed a more limited terpenoid profile in response to PHT. Under salt-free conditions, it produced guaiane-type sesquiterpenoids, as well as labdane-, cembrane-, colensane-, and clerodane-type diterpenoids. However, under 10% NaCl, only sesquiterpenoids were detected, indicating a narrower activation of terpenoid biosynthesis under saline stress.

Finally, an increased production of polyketides was also observed under PHT treatment, particularly in *S. thailandicus* and *N. triangularis*. In *S. thailandicus*, 2-pyrone derivatives and open-chain polyketides were detected under salt-free conditions, while acyl phloroglucinols were specific to the 10% NaCl condition. In *N. triangularis*, a broader diversity of polyketides was evident, including open-chain polyketides and macrolide lactones under both saline conditions. Additionally, monacolins and monacolin derivatives were detected exclusively under salt-free conditions, whereas 2-pyrone derivatives were specific to 10% NaCl.

Discussion

Deep sediment exploration in the GoM has revealed high fungal diversity at depths of 1,000-3,700 mbsl[4]. Here, we isolated three saprobic black yeasts - *S. thailandicus*, *N. triangularis*, and *N. salicorniae*, all members of the Dothideomycetes. To date, only two species are recognized within *Neophaeotheca* and *Salinomyces*[48,49]. Our findings document the presence of both *Neophaeotheca* species and one *Salinomyces* species in deep-sea sediments, expanding the known culturable fungal diversity of the GoM. Particularly, strain D9_S3_L1 exhibited high sequence similarity to the *N. salicorniae* CON1B8 isolate and to the *Nothophaeotheca mirabibensis* type strain. However, phylogenetic analyses resolved these taxa into

distinct clades. Therefore, based on morphology and strong sequence homology with the CON1B8 reference sequence, strain D9_S3_L1 was assigned to *N. salicorniae*, although further molecular and phenotypic analyses will be required to achieve definitive taxonomic resolution.

A defining feature of these black yeasts is their extreme halotolerance. While halotolerance had been previously reported for *N. triangularis*[45], this study provides evidence of halotolerance of *S. thailandicus* and *N. salicorniae*, placing them among the most halotolerant melanized fungi described to date, comparable to *H. werneckii* and *T. salinum*[7,8]. Optimal growth occurred between 3.5–10% NaCl, with reduced growth at higher salinities, consistent with trends reported in *H. werneckii* and *T. salinum*[50,51]. Although optical density is widely used to assess growth in black yeasts[31,51], fluctuations may reflect cell aggregation, morphological transitions, or cell death.

Salinity induced distinct, species-specific morphological responses. *S. thailandicus* shifted toward yeast-like growth, *N. triangularis* exhibited peripheral hyphal growth, and *N. salicorniae* maintained mixed morphologies. These responses parallel genotype-dependent morphologies described in *H. werneckii*[51]. However, limited genomic resources – currently available only for *S. thailandicus* and *N. triangularis*[52]–, preclude deeper genotype-phenotype analyses.

Black yeasts also display unconventional cell-division patterns[7]. Using low glucose concentrations, we observed yeast-like growth in *N. salicorniae* at 3.5% sea salt, contrasting with filamentous growth reported under glucose-rich conditions[7], indicating that carbon availability influences morphogenesis. In *N. triangularis*, salt concentration alone triggered morphological switching, and hyphae produced endoconidia internally, initiating distally and progressing toward the tip. These features highlight *N. triangularis* as a promising model for studying salt-responsive morphogenesis in black yeasts. *S. thailandicus*, although morphologically similar to *H. werneckii*[7,12], differed in its division mode, relying on unilateral and bilateral budding rather than fission.

Cell wall thickening is a well-recognized adaptive strategy in halotolerant and halophilic fungi to mitigate osmotic stress[21,50,53]. *S. thailandicus* exhibited the thickest walls, particularly under high salinity and melanin inhibition, while *N. triangularis* showed moderate thickening. Comparable thickening has been reported in *T. abietis*, where cell wall thickness ranged from 0.5–1 µm[50], and in *W. ichthyophaga*, which exhibited cell wall thickening up to 1.6 µm at high salinity (25% NaCl)[53]. In contrast, *N. salicorniae* showed no significant changes, resembling the behavior of *W. muriae* and *W. sebi*[53].

All three species produced DHN-melanin across salinities, as confirmed using melanin biosynthesis inhibitors. Genomic evidence in *S. thailandicus* supports DHN-melanin production (GenBank: TKA33268.1, TKA22391.1). With the recently released genome of *N. triangularis* (GenBank: BAAIJY000000000.1) and the forthcoming sequencing of *N. salicorniae*, it will be possible to evaluate the potential for synthesizing additional melanin types, as demonstrated in *Exophiala* spp.[47]

Melanin may also contribute to salt tolerance by reducing cell wall porosity. In all three species, melanin granules accumulated intra- and extracellularly and were reduced in size and abundance upon inhibitor treatment, consistent with observations in *H. werneckii* and *T. salinum*[16,50]. In *H. werneckii*, it has been proposed that melanin granules may limit cell wall permeability by reducing pore size[16]. While fungal cell wall porosity remains underexplored, the typical pore size in *Saccharomyces cerevisiae* is approximately 200 nm, increasing to 400 nm under oxidative stress[54]. In *Cryptococcus neoformans*, melanized cell walls are considerably less porous (4 nm) than non-melanized cell walls (10.6 nm)[55]. Melanin granules were frequently observed within cell wall pores in both *Neophaeotheca* species. Although it remains unclear whether these granules are synthesized in the cytoplasm and exported through these pores, or formed *in situ*, their presence supports the hypothesis that melanin may act as a physical barrier, reducing wall porosity and preventing glycerol loss, a key osmolyte in salt adaptation. Interestingly, TEM imaging also revealed translucent molecules traversing the cell wall, which we speculate to be glycerol. Given its low molecular weight (92.04 Da), glycerol is capable of diffusing passively across lipid bilayers, allowing cells to regulate its internal concentration in response to external osmotic pressure[16].

Although this is an exploratory metabolomic approach based on pooled samples for each species, the metabolomic analysis revealed noticeable species-specific differences in metabolite production in response to salinity and melanin inhibition. Fatty acids and terpenoids dominated across conditions, consistent with their central roles in primary metabolism and stress adaptation. In *Neophaeotheca* species, salt exposure shifted lipid profiles toward octadecanoids and lactones, whereas *Salinomyces* showed subtler but distinct metabolic changes. Shifts in octadecanoid production have previously been reported in other halotolerant black yeasts exposed to varying NaCl concentrations[56]. Two condition-specific fatty acid derivatives were consistently detected across species, suggesting conserved roles in osmotic stress responses: *N*-(carboxymethyl)-*N*,*N*-dimethyl-3-(tetradecanoylamino)propan-1-aminium was exclusively detected under salt-free conditions across all three black yeast species, whereas 18-hydroxyoctadeca-9,12-dienoic acid was uniquely present under 10% NaCl in *S. thailandicus* and *N. salicorniae*.

Notably, *N. triangularis* exhibited increased production of amino acid– and peptide-related metabolites under high salinity, a response well documented in plants[57] but, to our knowledge, not previously reported in black yeast. Additionally, aminocyclitols, a subclass of polyols, were detected in *S. thailandicus* and *N. triangularis*, representing a novel class of fungal osmoprotectants. Halotolerant yeasts synthesize polyols as part of their osmotic stress response[16]. Cyclitols, for example, are produced by halophytic plants and have been implicated in salt stress adaptation mechanisms[58]. Aminocyclitols have been predicted through *in silico* analyses to be potentially biosynthesized by fungi[59].

Inhibition of melanin biosynthesis by PHT profoundly altered the metabolomes of all three species, increasing both feature number and chemical diversity. Enhanced production of carbohydrates and fatty acid derivatives suggests compensatory mechanisms involving cell wall remodeling, thereby facilitating adaptation to hyperosmotic stress and potentially compensating for melanin loss, which serves a critical structural and protective function in the fungal cell wall. In *N. triangularis*, PHT treatment induced the synthesis of eicosanoids and oxylipins —molecules known to influence morphogenesis in other fungi — correlating with the observed inhibition of hyphal development and highlighting a link between melanin, lipid signaling, and morphogenesis.

In our study, PHT inhibited hyphal development, suggesting an important role for melanin in hyphal morphogenesis. Melanin has previously been reported to be associated with lipids[60]. Notably, *N. triangularis* produces several eicosanoid-derived oxylipins, including prostaglandins and thromboxanes. In fungi such as *Aspergillus*, *Ophiostoma*, and *Candida*, certain lipids, such as linoleic acid, eicosanoids like prostaglandins, and alkaloids such as polyamines, are known to influence morphogenesis and cellular differentiation[60-65], suggesting that these metabolites in the black yeasts may play essential roles in morphological adaptations to saline stress, particularly in *N. triangularis*, where this class of metabolites is especially prominent.

Most metabolites were detected in biomass-associated extracts (except for *N. triangularis* grown in salt-free medium), suggesting association with extracellular polymeric substances (EPS) that may form a protective matrix against osmotic stress. Overall, these black yeasts produced a diverse array of putative metabolites spanning lipid, terpenoid, alkaloid, carbohydrate, polyketide, amino acid, and peptide metabolism, with diversity markedly enhanced upon melanin inhibition.

Marine-derived fungi have garnered great interest due to their capacity to biosynthesize novel molecules with potential biotechnological applications[66]. Several metabolite classes identified here have

documented biotechnological potential, including nucleosides, xanthones, azaphilones, diterpenoids, alkaloids, and octadecanoids, among others.

Marine microorganisms are widely recognized as prolific sources of metabolites with diverse biological activities. In this study, *N. triangularis* was found to produce 9,12,13-trihydroxyoctadec-10-enoic acid, a metabolite with potential antifungal activity previously reported in the marine fungus *Emericellopsis cladophorae*[67], as well as spirostane steroids, a class of compounds previously described in *Neohelicomyces hyalosporus* and known for their cytotoxic activity[68]. In addition, several other classes of metabolites associated with marine fungi exhibiting confirmed biological activities were identified, including nucleosides with unique structural features and antibacterial properties[69,70], xanthones with antiviral and cytotoxic effects[66,71], azaphilones, colensane and clerodane diterpenoids with anti-inflammatory, antimicrobial, antitumor, and antiviral activities, as well as pyridine and carboline alkaloids capable of inducing apoptosis in small cell lung cancer cells and 2-pyrone derivatives with antibacterial activity[72-77]. Collectively, these findings highlight black yeasts as promising candidates for the discovery of novel molecules with potential biotechnological applications.

While the features reported here require further validation beyond *in silico* annotation using GNPS[36,39], SIRIUS[37], DEREPLICATOR[39], and MOLDISCOVERY[41] databases, our findings provide a valuable framework and resource for future investigations into the ecological roles and biotechnological potential of deep-sea black yeasts.

Conclusions

This study reports the presence of three black yeast species—*Salinomyces thailandicus*, *Neophaeotheca triangularis*, and *N. salicorniae*—in deep marine sediments from the Gulf of Mexico, highlighting their contribution to the region's fungal diversity. All three species exhibited morphological pleomorphisms, displaying either yeast-like or filamentous growth patterns, as well as changes in the cell division process and modifications in lipid and amino acid/peptide metabolism associated with salt stress responses. These findings suggest that these yeasts acquire substantial morphological and metabolomic plasticity when inhabiting marine environments and hypersaline waters, which are their commonly reported habitats.

The enhanced metabolite production observed under melanin synthesis inhibitory conditions highlights the role of melanin in conserving cellular energy, reaffirming its protective function in black yeasts. The metabolic pathways predominantly activated were those related to carbohydrates, lipids, terpenoids, and alkaloids, including a diverse array of metabolites with potential industrial applications.

Acknowledgements

Research was funded by the National Council of Science and Technology of Mexico—Mexican Ministry of Energy—Hydrocarbon Trust, project 201441. This is a contribution of the Gulf of Mexico Research Consortium (CIGoM). We thank the National Laboratory of Advanced Microscopy (LNMA) at the Centro de Investigación Científica y de Educación Superior de Ensenada (CICESE) for the use of the facilities. The authors thank Lluvia Vargas-Gastélum for her support in isolating the fungi and for creating the map in Figure 1, Ivonne Martínez-Mendoza for collecting the sediment samples during the XIXIM-7 campaign, Rodrigo Villanueva-Silva for his support with the initial metabolomic analysis, and Samantha V. González-Téllez for contributing to the graphical abstract figures. This work was partially supported by grants from UNAM-DGAPA PAPIIT IN203923 and FQ-PAIP 5000-9145 awarded to MF.

Maria Dolores Camacho-López was supported by a fellowship from the National Council of Humanities, Sciences, and Technologies (CONAHCyT, grant no. 315758).

We declare the use of ChatGPT only to improve the readability and proofreading of the manuscript.

Contributions: M.D.C.L contributed to conceptualization, investigation, writing the original draft, methodology, formal analysis, data curation, and editing; M. F. contributed with funding acquisition, writing, review and editing, data curation, and supervision; A.H.M. contributed with data curation, formal analysis, and writing, review and editing; M.R.: contributed to conceptualization, funding acquisition, writing, review and editing, formal analysis, supervision, project administration, and investigation.

Competing interests: All authors declare no competing interests.

References

1 Bik, H. M., Halanych, K. M., Sharma, J. & Thomas, W. K. Dramatic shifts in benthic microbial eukaryote communities following the Deepwater Horizon oil spill. *PloS one* **7**, e38550 (2012). https://doi.org/doi.org/10.1371/journal.pone.0038550

2 Herzka, S. Z., Zaragoza Álvarez, R. A., Peters, E. M., Hernández Cárdenas G. in *Atlas de línea base ambiental del golfo de México (tomo III, Segunda Parte), México: Consorcio de Investigación del Golfo de México.* (ed S. Z. Herzka) (México, 2021).

3 Yáñez-Arancibia, A. & Day, J. W. The Gulf of Mexico: towards an integration of coastal management with large marine ecosystem management. *Ocean & Coastal Management* **47**, 537-563 (2004). https://doi.org/10.1016/j.ocecoaman.2004.12.001

4 Vargas-Gastélum, L. *et al.* Targeted ITS1 sequencing unravels the mycodiversity of deep-sea sediments from the Gulf of Mexico. *Environmental Microbiology* **21**, 4046-4061 (2019). https://doi.org/10.1111/1462-2920.14754

5 Romero-Hernández, L. *et al.* Extra-heavy crude oil degradation by *Alternaria* sp. isolated from deep-sea sediments of the Gulf of Mexico. *Applied Sciences* **11**, 6090 (2021). https://doi.org/doi.org/10.3390/app11136090

6 Vélez, P., Gasca-Pineda, J. & Riquelme, M. Cultivable fungi from deep-sea oil reserves in the Gulf of Mexico: Genetic signatures in response to hydrocarbons. *Marine Environmental Research* **153**, 104816 (2020).

7 Mitchison-Field, L. M. *et al.* Unconventional cell division cycles from marine-derived yeasts. *Current Biology* **29**, 3439-3456. e3435 (2019). https://doi.org/doi.org/10.1101/657254

8 Gunde-Cimerman, N., Zalar, P., de Hoog, S. & Plemenitaš, A. Hypersaline waters in salterns–natural ecological niches for halophilic black yeasts. *FEMS Microbiology Ecology* **32**, 235-240 (2000). https://doi.org/doi.org/10.1111/j.1574-6941.2000.tb00716.x

9 Crous, P. W. *et al.* Fungal Planet description sheets: 400-468. *Persoonia* **36**, 316-458 (2016). https://doi.org/10.3767/003158516X692185

10 Selbmann, L. *et al.* Shed light in the dark lineages of the fungal tree of Life-STRES. *Life (Basel)* **10**, 362 (2020). https://doi.org/doi.org/10.3390/life10120362

11 Sterflinger, K. in *Biodiversity and Ecophysiology of Yeasts* (ed G. Péter, Rosa, C.) 501-514 (Springer, 2006).

12 Goshima, G. Growth and division mode plasticity is dependent on cell density in marine-derived black yeasts. *Genes to Cells* **27**, 124-137 (2022). https://doi.org/10.1111/gtc.12916

13 Gunde-Cimerman, N. & Plemenitaš, A. in *Life in Extreme Environments* Chapter 11, 177-185 (2006).

14 Gunde-Cimerman, N., Plemenitas, A. & Oren, A. Strategies of adaptation of microorganisms of the three domains of life to high salt concentrations. *FEMS Microbiology Reviews* **42**, 353-375 (2018). https://doi.org/10.1093/femsre/fuy009

15 Kogej, T., Wheeler, M. H., Lanisnik Rizner, T. & Gunde-Cimerman, N. Evidence for 1,8-dihydroxynaphthalene melanin in three halophilic black yeasts grown under saline and non-saline conditions. *FEMS Microbiology Letters* **232**, 203-209 (2004). https://doi.org/10.1016/S0378-1097(04)00073-4

16 Kogej, T. *et al.* Osmotic adaptation of the halophilic fungus *Hortaea werneckii*: role of osmolytes and melanization. *Microbiology* **153**, 4261-4273 (2007). https://doi.org/doi.org/10.1099/mic.0.2007/010751-0

17 Camacho, E. *et al.* The structural unit of melanin in the cell wall of the fungal pathogen *Cryptococcus neoformans*. *Journal of Biological Chemistry* **294**, 10471-10489 (2019). https://doi.org/doi.org/10.1074/jbc.RA119.008684

18 Pralea, I. E. *et al.* From extraction to advanced analytical methods: The challenges of melanin analysis. *International Journal of Molecular Sciences* **20**, 3943 (2019). https://doi.org/doi.org/10.3390/ijms20163943

19 Cao, W. *et al.* Unraveling the structure and function of melanin through synthesis. *Journal of the American Chemical Society* **143**, 2622-2637 (2021). https://doi.org/doi.org/10.1021/jacs.0c12322

20 Pal, A. K., Gajjar, D. U. & Vasavada, A. R. DOPA and DHN pathway orchestrate melanin synthesis in *Aspergillus* species. *Medical Mycology* **52**, 10-18 (2014). https://doi.org/doi.org/10.3109/13693786.2013.826879

21 Jiménez-Gómez, I. *et al.* Surviving in the brine: A multi-omics approach for understanding the physiology of the halophile fungus *Aspergillus sydowii* at saturated NaCl concentration. *Frontiers in Microbiology* **13**, 840408 (2022). https://doi.org/10.3389/fmicb.2022.840408

22 Agrawal, S., Chavan, P. & Dufosse, L. Hidden treasure: Halophilic fungi as a repository of bioactive lead compounds. *Journal of Fungi* **10** (2024). https://doi.org/doi.org/10.3390/jof10040290

23 Gadanho, M., Almeida, J. M. & Sampaio, J. P. Assessment of yeast diversity in a marine environment in the south of Portugal by microsatellite-primed PCR. *Antonie van Leeuwenhoek* **84**, 217-227 (2003). https://doi.org/doi.org/10.1023/a:1026038213195

24 Gardes, M. & Bruns, T. D. ITS primers with enhanced specificity for basidiomycetes-application to the identification of mycorrhizae and rusts. *Molecular Ecology* **2**, 113-118 (1993). https://doi.org/10.1111/j.1365-294X.1993.tb00005.x

25 White, T. J., Bruns, T., Lee, S. & Taylor, J. Amplification and direct sequencing of fungal ribosomal RNA genes for phylogenetics. *PCR protocols: a guide to methods and applications* **18**, 315-322 (1990).

26 Kurtzman, C. P. & Robnett, C. J. Identification and phylogeny of ascomycetous yeasts from analysis of nuclear large subunit (26S) ribosomal DNA partial sequences. *Antonie van Leeuwenhoek* **73**, 331-371 (1998). https://doi.org/doi.org/10.1023/a:1001761008817

27 Kumar, S. *et al.* MEGA12: Molecular Evolutionary Genetic Analysis version 12 for adaptive and green computing. *Molecular Biology and Evolution* **41**, msae263 (2024).

28 Benson, D. A. *et al.* GenBank. *Nucleic Acids Research* **41**, D36-D42 (2012). https://doi.org/https://doi.org/10.1093/nar/gks1195

29 Tamura, K. & Nei, M. Estimation of the number of nucleotide substitutions in the control region of mitochondrial DNA in humans and chimpanzees. *Molecular Biology and Evolution* **10**, 512-526 (1993).

30 Atlas, R. M. *The handbook of microbiological media for the examination of food*. (CRC press, 2006).

31 Kejzar, A., Gobec, S., Plemenitas, A. & Lenassi, M. Melanin is crucial for growth of the black yeast *Hortaea werneckii* in its natural hypersaline environment. *Fungal Biology* **117**, 368-379 (2013). https://doi.org/10.1016/j.funbio.2013.03.006

32 Hickey, P. C., Swift, S. R., Roca, M. G. & Read, N. D. in *Microbial Imaging Methods in Microbiology* 63-87 (2004).

33 Schindelin, J. *et al.* Fiji: an open-source platform for biological-image analysis. *Nature Methods* **9**, 676-682 (2012). https://doi.org/doi.org/10.1038/nmeth.2019

34 Gniewosz, M. & Duszkiewicz-Reinhard, W. Comparative studies on pullulan synthesis, melanin synthesis and morphology of white mutant *Aureobasidium pullulans* B-1 and parent strain A.p.-3. *Carbohydrate Polymers* **72**, 431-438 (2008). https://doi.org/10.1016/j.carbpol.2007.09.009

35 Schmid, R. *et al.* Integrative analysis of multimodal mass spectrometry data in MZmine 3. *Nature Biotechnology* **41**, 447-449 (2023). https://doi.org/doi.org/10.1038/s41587-023-01690-2

36 Nothias, L. F. *et al.* Feature-based molecular networking in the GNPS analysis environment. *Nature Methods* **17**, 905-908 (2020). https://doi.org/10.1038/s41592-020-0933-6

37 Dührkop, K. *et al.* SIRIUS 4: a rapid tool for turning tandem mass spectra into metabolite structure information. *Nature Methods* **16**, 299-302 (2019). https://doi.org/doi.org/10.1038/s41592-019-0344-8

38 Hernández-Melgar, A. G., Guerrero, A. & Moreno-Ulloa, A. Chronic exposure to petroleum-derived hydrocarbons alters human skin microbiome and metabolome profiles: A pilot study. *Journal of Proteome Research* **23**, 4273-4285 (2024). https://doi.org/10.1021/acs.jproteome.4c00256

39 Aron, A. T. *et al.* Reproducible molecular networking of untargeted mass spectrometry data using GNPS. *Nature Protocols* **15**, 1954-1991 (2020). https://doi.org/doi.org/10.1038/s41596-020-0317-5

40 Sumner, L. W. *et al.* Proposed minimum reporting standards for chemical analysis: chemical analysis working group (CAWG) metabolomics standards initiative (MSI). *Metabolomics* **3**, 211-221 (2007). https://doi.org/doi.org/10.1007/s11306-007-0082-2

41 Cao, L. *et al.* MolDiscovery: learning mass spectrometry fragmentation of small molecules. *Nature Communications* **12**, 3718 (2021). https://doi.org/doi.org/10.1038/s41467-021-23986-0

42 Dührkop, K., Shen, H., Meusel, M., Rousu, J. & Böcker, S. Searching molecular structure databases with tandem mass spectra using CSI: FingerID. *Proceedings of the National Academy of Sciences* **112**, 12580-12585 (2015).

43 Mohimani, H. *et al.* Dereplication of microbial metabolites through database search of mass spectra. *Nature Communications* **9**, 4035 (2018). https://doi.org/doi.org/10.1038/s41467-018-06082-8

44 Dührkop, K. *et al.* Systematic classification of unknown metabolites using high-resolution fragmentation mass spectra. *Nature Biotechnology* **39**, 462-471 (2021). https://doi.org/doi.org/10.1038/s41587-020-0740-8

45 Chung, D., Kim, H. & Choi, H. S. Fungi in salterns. *Journal of Microbiology* **57**, 717-724 (2019). https://doi.org/doi.org/10.1007/s12275-019-9195-3

46 Kogej, T. *et al.* Osmotic adaptation of the halophilic fungus *Hortaea werneckii*: role of osmolytes and melanization. *Microbiology* **153**, 4261-4273 (2007).

47 Carr, E. C. *et al.* Characterization of a novel polyextremotolerant fungus, *Exophiala viscosa*, with insights into its melanin regulation and ecological niche. *G3 Genes|Genomes|Genetics* **13**, 1-37 (2023). https://doi.org/10.1093/g3journal/jkad110

48 Czachura, P., Owczarek-Kościelniak, M. & Piątek, M. *Salinomyces polonicus*: A moderately halophilic kind of the most extremely halotolerant fungus *Hortaea werneckii*. *Fungal Biology* **125**, 459-468 (2021). https://doi.org/doi.org/10.1016/j.funbio.2021.01.003

49 Abdollahzadeh, J., Groenewald, J. Z., Coetzee, M. P. A., Wingfield, M. J. & Crous, P. W. Evolution of lifestyles in Capnodiales. *Studies in Mycology* **95**, 381-414 (2020). https://doi.org/10.1016/j.simyco.2020.02.004

50 Kogej, T., Gorbushina, A. A. & Gunde-Cimerman, N. Hypersaline conditions induce changes in cell-wall melanization and colony structure in a halophilic and a xerophilic black yeast species of the genus *Trimmatostroma*. *Mycological Research* **110**, 713-724 (2006). https://doi.org/10.1016/j.mycres.2006.01.014

51 Zalar, P. *et al.* The extremely halotolerant black yeast *Hortaea werneckii* - a model for intraspecific hybridization in clonal fungi. *IMA Fungus* **10**, 1-27 (2019). https://doi.org/10.1186/s43008-019-0007-5

52 Coleine, C. *et al.* Peculiar genomic traits in the stress-adapted cryptoendolithic Antarctic fungus *Friedmanniomyces endolithicus*. *Fungal Biology* **124**, 458-467 (2020). https://doi.org/doi.org/10.1016/j.funbio.2020.01.005

53 Kralj Kuncic, M., Kogej, T., Drobne, D. & Gunde-Cimerman, N. Morphological response of the halophilic fungal genus *Wallemia* to high salinity. *Applied Environmental Microbiology* **76**, 329-337 (2010). https://doi.org/10.1128/AEM.02318-09

54 de Souza Pereira, R. & Geibel, J. Direct observation of oxidative stress on the cell wall of *Saccharomyces cerevisiae* strains with atomic force microscopy. *Molecular and Cellular Biochemistry* **201**, 17-24 (1999). https://doi.org/10.1023/a:1007007704657

55 Jacobson, E. S. & Ikeda, R. Effect of melanization upon porosity of the cryptococcal cell wall. *Medical Mycology* **43**, 327-333 (2005). https://doi.org/10.1080/13693780412331271081

56 Turk, M. *et al.* Salt-induced changes in lipid composition and membrane fluidity of halophilic yeast-like melanized fungi. *Extremophiles* **8**, 53-61 (2004). https://doi.org/10.1007/s00792-003-0360-5

57 Heidarzadeh, A. Role of amino acids in plant growth, development, and stress responses: A comprehensive review. *Discover Plants* **2**, 1-31 (2025).

58 Derkaczew, M., Martyniuk, P., Osowski, A. & Wojtkiewicz, J. Cyclitols: From basic understanding to their association with neurodegeneration. *Nutrients* **15**, 2029 (2023). https://doi.org/doi.org/10.3390/nu15092029

59 Mahmud, T. Progress in aminocyclitol biosynthesis. *Current opinion in chemical biology* **13**, 161-170 (2009).

60 Chrissian, C. *et al.* Solid-state NMR spectroscopy identifies three classes of lipids in *Cryptococcus neoformans* melanized cell walls and whole fungal cells. *Journal of Biological Chemistry* **295**, 15083-15096 (2020). https://doi.org/10.1074/jbc.RA120.015201

61 Koroleva, E. *et al.* Exploring polyamine metabolism of the yeast-like fungus, *Emergomyces africanus*. *FEMS Yeast Research* **24**, foae038 (2024).

62 Niu, M. *et al.* Fungal oxylipins direct programmed developmental switches in filamentous fungi. *Nature Communications* **11**, 5158 (2020). https://doi.org/10.1038/s41467-020-18999-0

63 Naruzawa, E. S., Malagnac, F. & Bernier, L. Effect of linoleic acid on reproduction and yeast–mycelium dimorphism in the Dutch elm disease pathogens. *Botany* **94**, 31-39 (2016). https://doi.org/10.1139/cjb-2015-0156

64 Kupfahl, C., Tsikas, D., Niemann, J., Geginat, G. & Hof, H. Production of prostaglandins, isoprostanes and thromboxane by *Aspergillus fumigatus*: Identification by gas chromatography–tandem mass spectrometry and quantification by enzyme immunoassay. *Molecular Immunology* **49**, 621-627 (2012).

65 Noverr, M. C. & Huffnagle, G. B. Regulation of *Candida albicans* morphogenesis by fatty acid metabolites. *Infection and Immunity* **72**, 6206-6210 (2004). https://doi.org/10.1128/IAI.72.11.6206-6210.2004

66 Yurchenko, A. N., Girich, E. V. & Yurchenko, E. A. Metabolites of marine sediment-derived fungi: actual trends of biological activity studies. *Marine Drugs* **19**, 88 (2021).

67 Goncalves, M. F. M., Hilario, S., Van de Peer, Y., Esteves, A. C. & Alves, A. Genomic and metabolomic analyses of the marine fungus *Emericellopsis cladophorae*: Insights into saltwater adaptability mechanisms and its biosynthetic potential. *Journal of Fungi* **8** (2021). https://doi.org/10.3390/jof8010031

68 Zheng, W., Han, L., He, Z. J. & Kang, J. C. New spirostane from a fungus *Neohelicomyces hyalosporus* and its bioactivity. *Chemistry & Biodiversity* **20**, e202300313 (2023).

69 Chen, M., Fu, X.-M., Kong, C.-J. & Wang, C.-Y. Nucleoside derivatives from the marine-derived fungus Aspergillus versicolor. *Natural Product Research* **28**, 895-900 (2014).

70 Huang, R.-M. *et al.* Marine nucleosides: Structure, bioactivity, synthesis and biosynthesis. *Marine Drugs* **12**, 5817-5838 (2014).

71 Liu, F.-a. *et al.* Xanthones and quinolones derivatives produced by the deep-sea-derived fungus *Penicillium* sp. SCSIO Ind16F01. *Molecules* **22**, 1999 (2017).

72 Amin, M., Liang, X., Ma, X., Dong, J.-D. & Qi, S.-H. New pyrone and cyclopentenone derivatives from marine-derived fungus *Aspergillus sydowii* SCSIO 00305. *Natural Product Research* **35**, 318-326 (2021).

73 Zhou, X.-M. *et al.* Antibacterial α-pyrone derivatives from a mangrove-derived fungus *Stemphylium* sp. 33231 from the South China Sea. *The Journal of Antibiotics* **67**, 401-403 (2014).

74 Chen, S. *et al.* Tersaphilones AE, cytotoxic chlorinated azaphilones from the deep-sea-derived fungus *Phomopsis tersa* FS441. *Tetrahedron* **78**, 131806 (2021).

75 Shi, Q. *et al.* Diterpenoids of marine organisms: isolation, structures, and bioactivities. *Marine Drugs* **23**, 131 (2025).

76 Hu, Y. *et al.* Cytotoxic pyridine alkaloids from a marine-derived fungus *Arthrinium arundinis* exhibiting apoptosis-inducing activities against small cell lung cancer. *Phytochemistry* **213**, 113765 (2023).

77 Hao, M.-J. *et al.* β-Carboline alkaloids from the deep-sea fungus *Trichoderma* sp. MCCC 3A01244 as a new type of anti-pulmonary fibrosis agent that inhibits TGF-β/smad signaling pathway. *Frontiers in Microbiology* **13**, 947226 (2022).

78 Ryan, W. B. *et al.* Global multi-resolution topography synthesis. *Geochemistry, Geophysics, Geosystems* **10** (2009).

Tables

Table 1. Molecular identification of black yeast species isolated from deep-sea sediments of the Gulf of Mexico.

Station Depth (bsl)	Species	Molecular marker	Coverage (%)	Identity %	GenBank acc. No./ strain	
E33 3,435 m	***Salinomyces thailandicus***	ITS	100	100	NR_171710.1/ CBS 125423^{*T}	PV583351/P 2_F1_L1**
		D1/D2	100	100	NG_057846.1/ CBS 125423^{*T}	PV583355/P 2_F1_L1**
C23 3,739 m	***Neophaeotheca triangularis***	ITS	92	100	NR_137142.1/ CBS 471.90^{*T}	PV583352/ D1_F4_L1**
		D1/D2	100	100	MH873909.1/ CBS 471.90^{*T}	PV583356/ D1_F4_L1**
TS1 2,417 m	***Neophaeotheca salicorniae***	ITS	93	98.97	MN309703.1/ CON1B8*	PV583353/ D9_S3_L1**
		D1/D2	98	100	MN307928.1/ CON1B8*	PV583357/ D9_S3_L1**

* Strains of reference; ** strains of this study; ^{T}Type strain.

Table 2. Average sizes of the different cells produced by black yeasts at varying salt concentrations on Czapek solid medium.

Species	Cell morphology	Sea salt		NaCl	
		0	3.5%	10%	20%
S. thailandicus	Unilateral	5.2 x 2.5	5.1 x 2.4	4.5 x 2.2	4.3 x 2.2
	Bilateral	7.7 x 3.2	7.6 x 2.9	6.3 x 2.6	6.6 x 2.5
N. triangularis	Aseptate endoconidium	5.6 x 5.0	5.10 x 5.0	5.0 x 4.2	5.6 x 5.1
	Septate endoconidium	8.7 x 6.2	7.2 x 5.3	6.6 x 5.1	8.1 x 6.5
	Muriform cell	11.2 x 7	9.3 x 6.5	9.9 x 7.4	10.7 x 7
N. salicorniae	Aseptate endoconidium	5.1 x 4.8	5.10 x 4.6	5.2 x 5.0	
	Septate endoconidium	7 x 5.4	7.2 x 5.6	7.1 x 5.7	
	Muriform cell	8.4 x 6.1	9.0 x 6.5	9.9 x 6.6	

Measurements (length x width) in µm.

Table 3. Putative metabolite classes produced by black yeasts under different stress conditions.

Class	*S. thailandicus*				*N. triangularis*				*N. salicorniae*			
PHT	-		+		-		+		-		+	
NaCl (%)	**0**	**10**	**0**	**10**	**0**	**10**	**0**	**10**	**0**	**10**	**0**	**10**
Polyamines	F1	F18	F32				F157		F87		F431	
Pyridine alkaloids	F2					F123	F144				F435	F472
Tripeptides	F6	F20			F88	F124	F163	F276	F390			F477
Cyclitols	F7											
Amino cyclitols				F78		F133						
Monosaccharides	F34						F169	F281				F481
Disaccharides			F33	F70			F170	F279			F479	
Unsaturated fatty acids					F108			F335				
Unsaturated fatty acids (Linoleic acid)							F230	F357				
Hydroxy fatty acids							F177	F300				
Epoxy fatty acids									F402			
Epoxy fatty acids			F50		F107		F209	F352	F408		F457	
Other Octadecanoids					F106		F198					
Other Octadecanoids				F81				F360	F406			
Other Octadecanoids					F97	F134		F307	F396			
Jasmonic acids							F200					
Prostaglandins							F202					
Thromboxanes							F196	F311				
Rhamnolipids							F195					
Sophorolipids								F341				
Sphingoid bases							F211					
Acetogenins		F27										
Monoacylglycerols							F203	F345	F401		F453	F492
Glycerophosphocholines					F109							

F1 to F492 refer to IDs listed in Supplementary Data 2, which contains supplementary information related to metabolomic data acquisition.

Figure captions

Figure 1. Sampling sites and isolation locations of black yeasts in the Gulf of Mexico.

The sampling sites where black yeasts were isolated are marked with white circles. *Salinomyces thailandicus* was isolated from site E33, *Neophaeotheca triangularis* from site C23, and *Neophaeotheca salicorniae* from site TS1. Map generated using GeoMapApp (www.geomapapp.org) under a CC BY[78] license.

Figure 2. Black yeasts halotolerance.

Pigmented colonies (3 per plate) were grown for 90 days on modified Czapek dox medium containing different salt concentrations. *Sth- Salinomyces thailandicus, Ntr- Neophaeotheca triangularis,* and *Nsa- N. salicorniae.* Scale bar = 10 mm.

Figure 3. Salinity effects on the morphology and growth of black yeasts.

As the salt concentration increases, **A**. *S. thailandicus* shifts from filamentous to yeast-like growth, **B.** *N. triangularis* shifts from yeast-like growth to filamentous growth, **C**. *N. salicorniae* exhibits both yeast-like and filamentous growth. Colony without salt and with 10% NaCl close-ups (63X) show filamentous or yeast-like morphology (arrows). **D.** *S. thailandicus,* **E***. N. triangularis, and* **F.** *N. salicorniae* growth measured by optical density (OD_{600}). Scale bar = 5 mm. Data were analyzed using one-way ANOVA followed by Tukey's multiple comparisons test.

Figure 4. Morphology and cell division patterns observed by light microscopy.

A. Cell morphology patterns of *S. thailandicus* (without salt): **a**. Yeast-like cell; **b**. Unilateral budding; **c**. Bilateral budding; **d-e**. Meristematic cell; **f**. Filamentous growth; **g**. Colony. **B.** In *S. thailandicus,* budding was the main cell division pattern, and hyphae formation was observed on 10% NaCl (arrows). **C**. *S. thailandicus* cell division record. **D.** Cell morphology patterns of *N. triangularis* (without salt): **a.** Aseptate endoconidium; **b.** Septate endoconidium; **c.** Muriform cell; **d.** Meristematic clumped cells; **e.** Endoconidium release; **f.** Hyphae (10% NaCl); **g.** Endoconidium production within hyphae (10% NaCl)**. E.** *N. triangularis* endoconidiation was the predominant cell division pattern, and hyphae formation was observed on 10% NaCl (arrows). **F**. *N. triangularis* cell division record. **G.** Cell morphology patterns of *N. salicorniae* (without salt) **a.** Aseptate endoconidium; **b.** Septate endoconidium; **c.** Muriform cell **d.** Meristematic clumped cells; **e.** Hyphal cell; **f.** Melanized colony **g.** A melanized colony with the cell wall stained with calcofluor white. **H**. *N. salicorniae* endoconidiation was the predominant cell division pattern, and hyphae formation was observed without NaCl (arrows). **I**. *N. salicorniae* cell division record. Time-lapse in h:min. Scale bar = 10 µm. Statistically significant differences are indicated (**P* < 0.05; ***P* < 0.01; *****P* < 0.0001), bars indicate standard deviation.

Figure 5. Effects of melanin inhibitors on growth and cell morphology.

A. Determination of DOPA or DHN-melanin production with kojic acid (KA) and phthalide (PHT) inhibitors. Arrows show PHT inhibiting concentrations. **B.** Representative image on Czapek medium with 10% NaCl shows phthalide effect on non-production of hyphae, instead of clumps cells were formed (arrows). PHT + and –, with and without phthalide. *Sth* = *S. thailandicus*, *Ntr* = *N. triangularis*, *Nsa* = *N. salicorniae*. Scale bar = 10 µm.

Figure 6. Effects of salinity and melanin inhibitor phthalide (PHT) on cell wall (CW) thickness.

S. thailandicus (left)*, N. triangularis* (middle)*,* and *N. salicorniae* (right) cells. **A.** Melanin accumulation (M). **B.** Black yeast cells wall close-ups showing melanin granules accumulation and other molecules (arrows), probably glycerol. 0 and 10%, without and with NaCl. PHT + and –, with and without phthalide. Images obtained by transmission electron microscopy (TEM); scale bar = 1 µm. **C.** Cell wall thickness. Statistically significant differences are marked (**P* < 0.05; ***P* < 0.01; *****P* < 0.0001), bars indicate standard deviation. One-way ANOVA and Tukey's multiple comparisons test were used to analyze the data.

Figure 7. Cell surface features of melanized cells of black yeasts.

Accumulation of melanin granules outside or within the cell wall is indicated by arrows in bright-field (BF) and scanning electron microscopy (SEM) images. In *S. thailandicus*, melanin and other molecules, as well as the translocation of melanin through pores in the cell wall of *Neophaeotheca* species, are highlighted with arrows in the close-up sections of transmission electron microscopy (TEM) micrographs. *Sth* = *S. thailandicus*, *Ntr* = *N. triangularis*, *Nsa* = *N. salicorniae*. BF = Bright-field microscopy (scale bar = 5 µm); SEM and TEM = Scanning and transmission electron microscopy, respectively (scale bar = 1.0 µm, TEM magnifications = 0.5 µm).

Figure 8. Differences in the metabolic profiles of black yeasts exposed to varying salt concentrations and the melanin biosynthesis inhibitor phthalide (PHT), analyzed using untargeted metabolomic and chemoinformatic approaches.

(A) The donut chart illustrates the predominant metabolic pathways, while (B) the heatmap presents the chemical superclasses of putative metabolites, assigned to MS2-containing features detected across all experimental groups. The scale of colors pink to black in B indicates the number of identified features at each superclass level. Chemical classification was conducted using CANOPUS via NPClassifier.

Editorial Summary:

Black yeasts from deep-sea sediments exhibit species-specific morphogenetic and metabolomic responses to salinity and melanin inhibition. Fatty acid-rich profiles, carbohydrates, and amino acid accumulation suggest osmotic stress adaptations.

Peer Review Information:

Communications Biology thanks Louisi Souza de Oliveira, Federico Laich and the other, anonymous, reviewer(s) for their contribution to the peer review of this work. Primary Handling Editors: Linn Hoffmann and Tobias Goris.

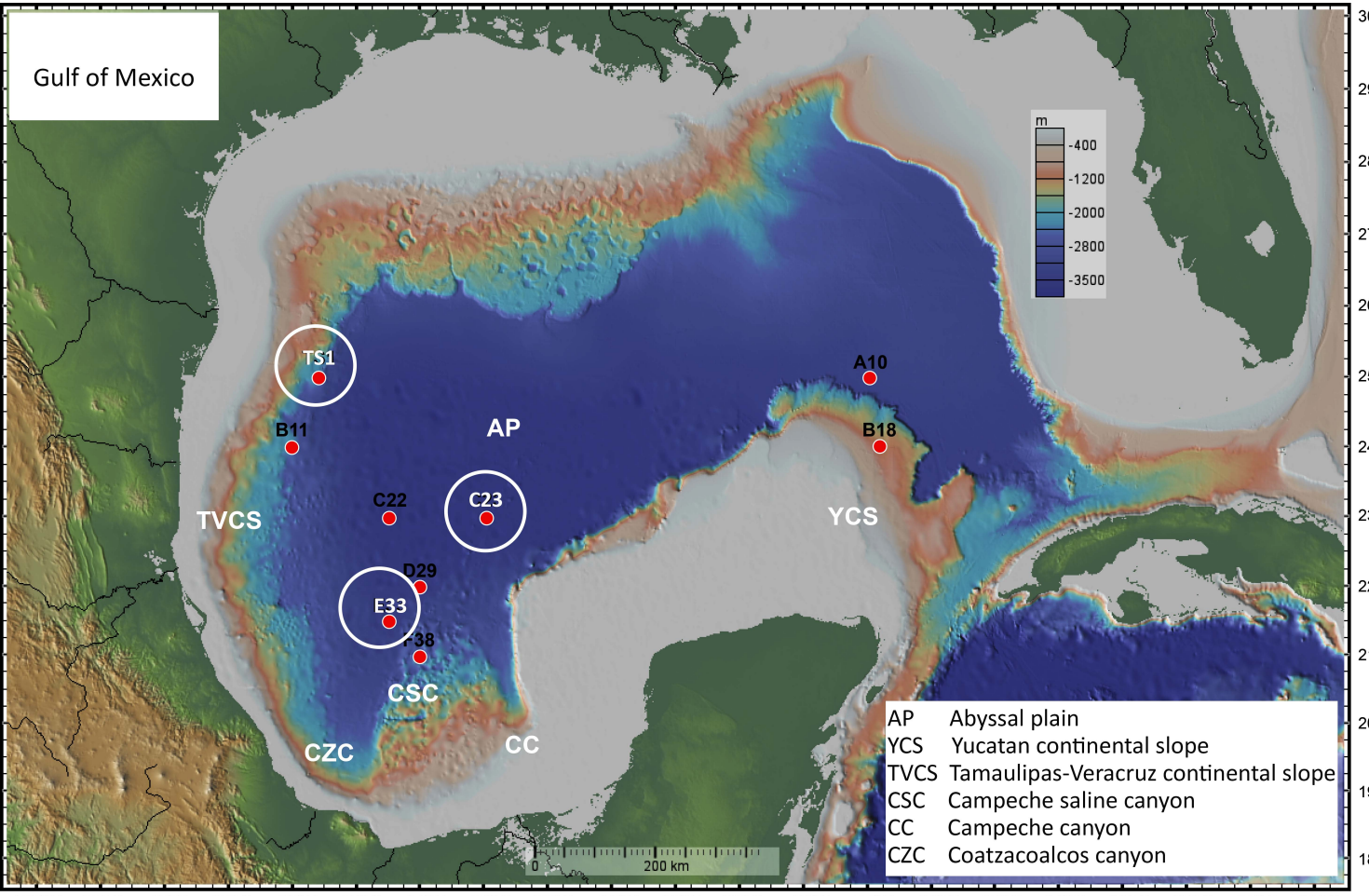
Gulf of Mexico
m
-400
-1200
-2000
-2800
-3500
TS1
B11
A10
B18
C22
C23
D29
E33
F38
AP
TVCS
YCS
CSC
CZC
CC
AP Abyssal plain
YCS Yucatan continental slope
TVCS Tamaulipas-Veracruz continental slope
CSC Campeche saline canyon
CC Campeche canyon
CZC Coatzacoalcos canyon
0
200 km
30°N
29°N
28°N
27°N
26°N
25°N
24°N
23°N
22°N
21°N
20°N
19°N
18°N
100°W
99°W
98°W
97°W
96°W
95°W
94°W
93°W
92°W
91°W
90°W
89°W
88°W
87°W
86°W
85°W
84°W
83°W
82°W
81°W
80°W

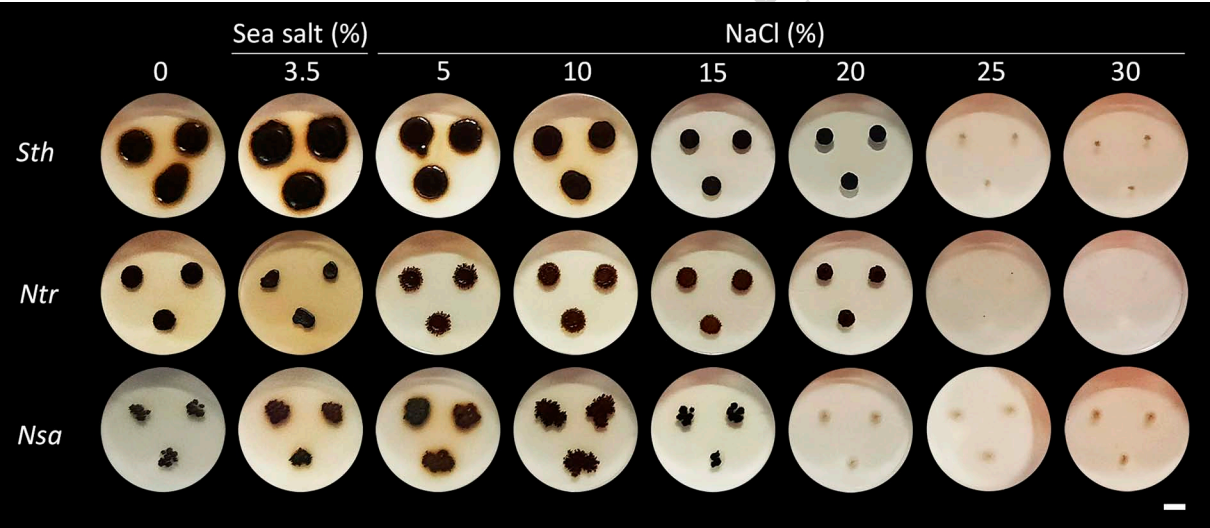

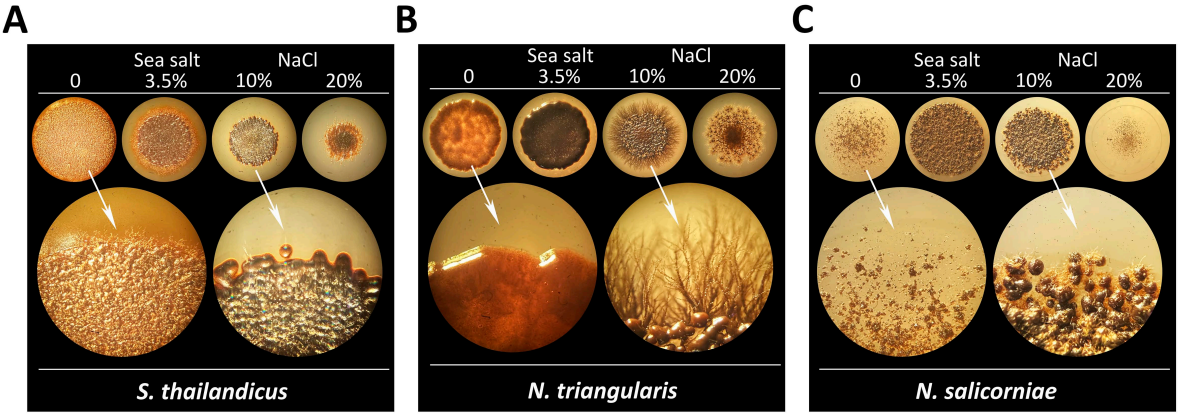
A
B
C
Sea salt
NaCl
0
3.5%
10%
20%
S. thailandicus
N. triangularis
N. salicorniae

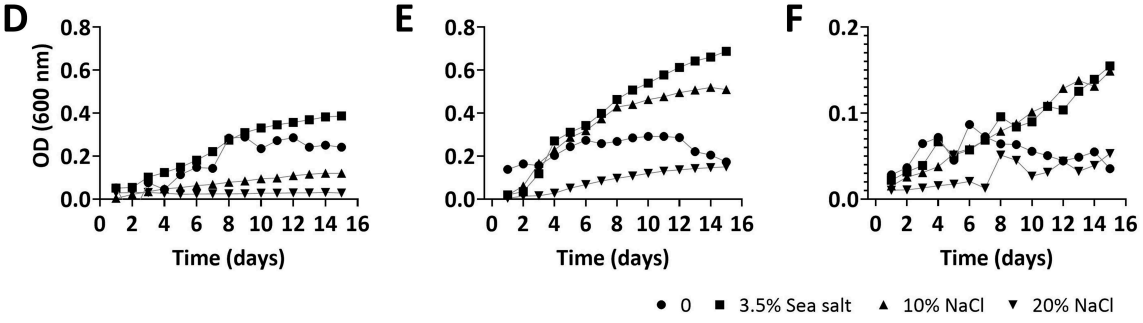
D
E
F
OD (600 nm)
Time (days)
0
3.5% Sea salt
10% NaCl
20% NaCl

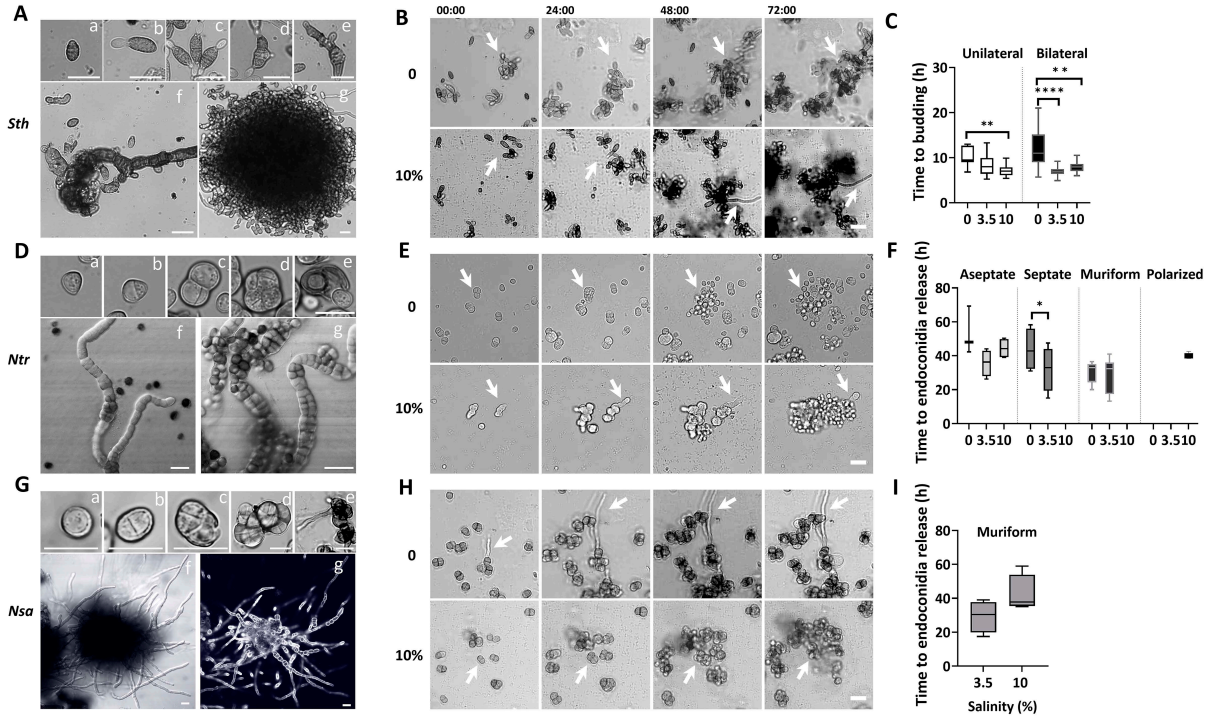
A
B
C
D
E
F
G
H
I
Sth
Ntr
Nsa
00:00
24:00
48:00
72:00
0
10%
Unilateral
Bilateral
Time to budding (h)
0 3.5 10
Aseptate
Septate
Muriform
Polarized
Time to endoconidia release (h)
0 3.5 10
Salinity (%)

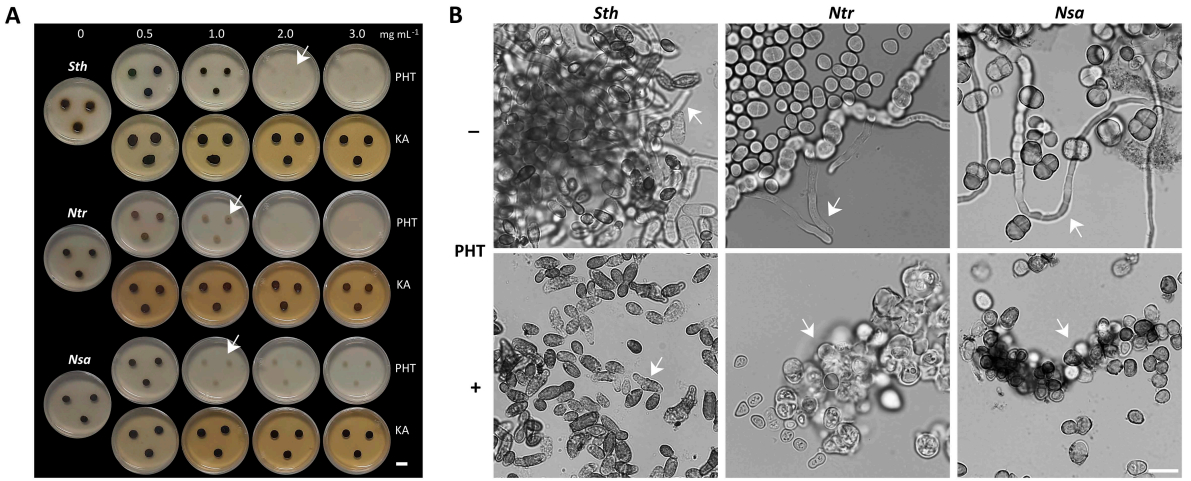

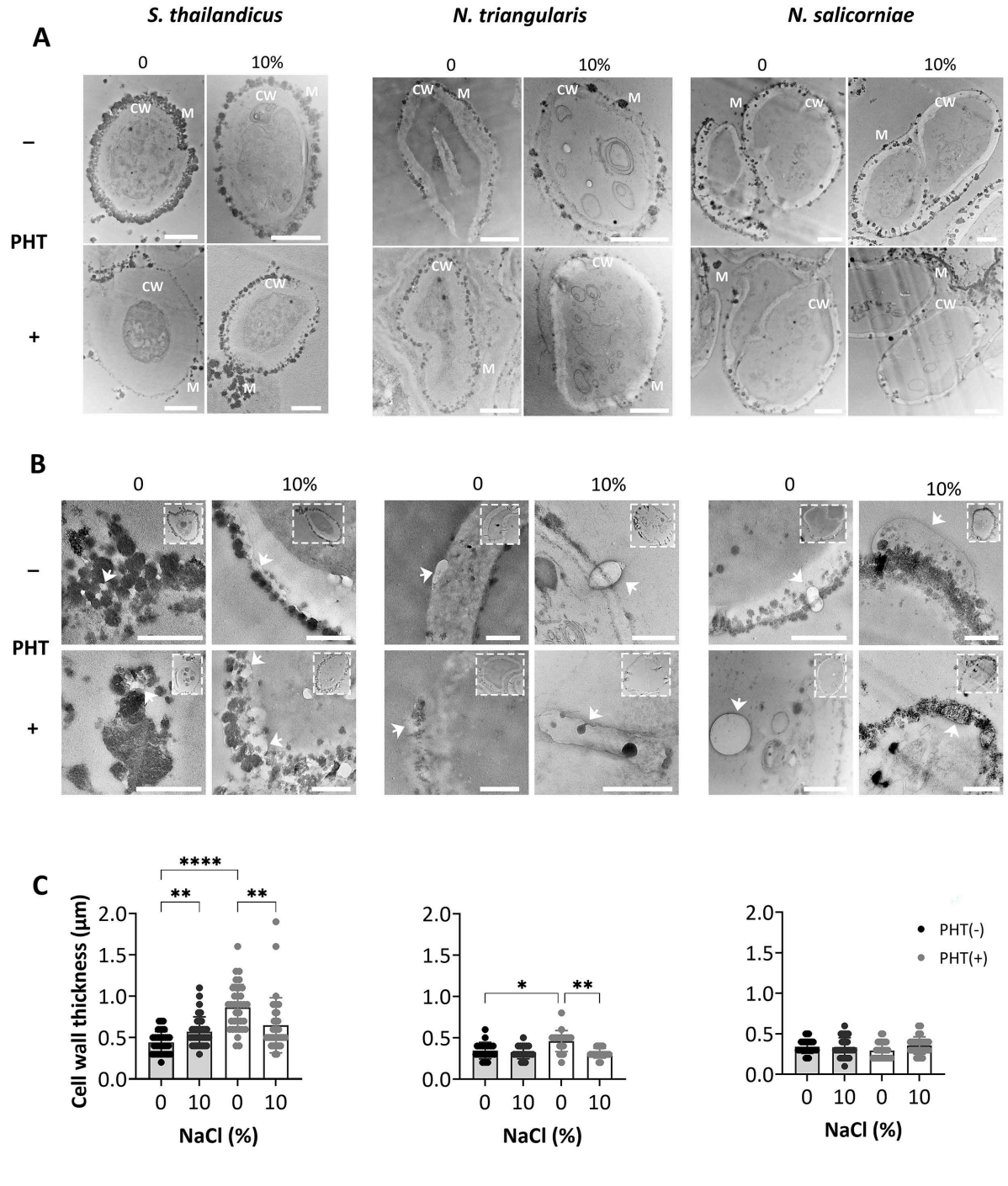
A
S. thailandicus
N. triangularis
N. salicorniae
0
10%
–
PHT
+
CW
M
B
C
Cell wall thickness (µm)
NaCl (%)
PHT(-)
PHT(+)
****
**
*

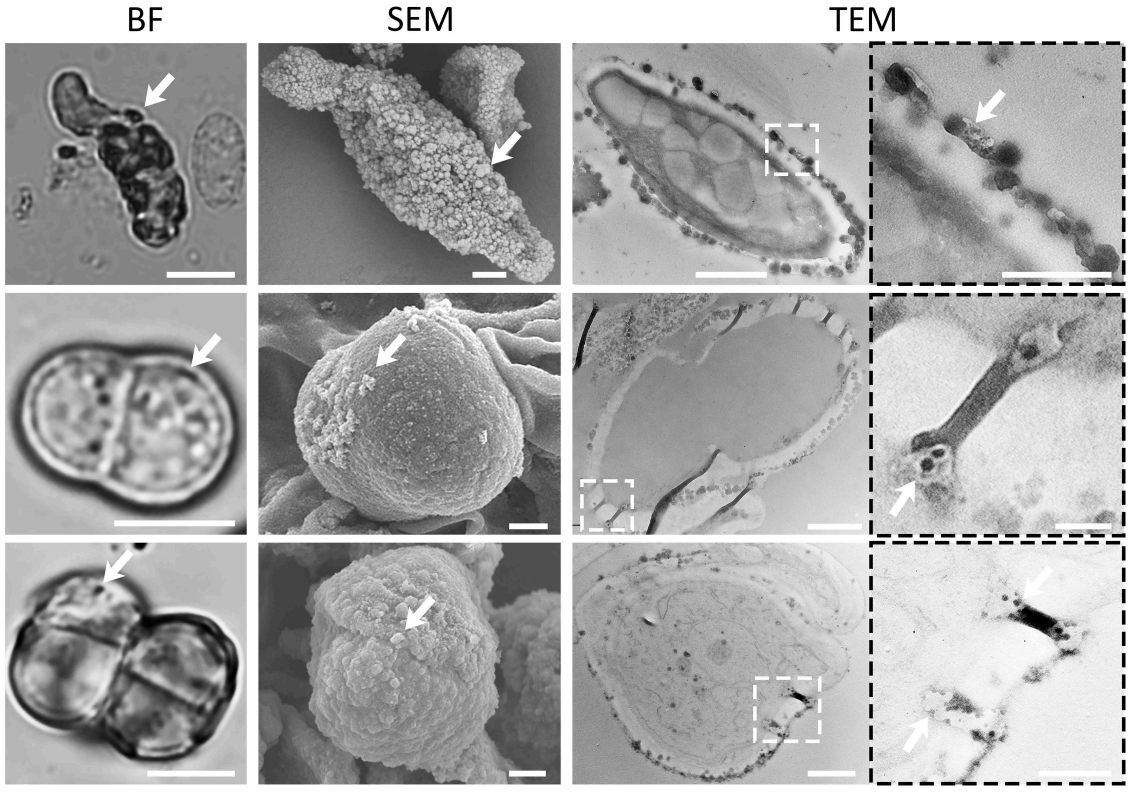
BF
SEM
TEM
Sth
Ntr
Nsa


A
S. thailandicus
N. triangularis
N. salicorniae
NaCl
0
10%
PHT
–
+
15 features
36 features
20 features
21 features
118 features
125 features
31 features
11 features
43 features
32 features
Fatty acids
Alkaloids
Amino acids and Peptides
Carbohydrates
Polyketides
Shikimates and Phenylpropanoids
Terpenoids
B
Eicosanoids
Fatty Acids and Conjugates
Fatty acyl glycosides
Fatty acyls
Fatty amides
Fatty esters
Glycerolipids
Glycerophospholipids
Octadecanoids
Sphingolipids
Anthranilic acid alkaloids
Guanidine alkaloids
Histidine alkaloids
Lysine alkaloids
Nicotinic acid alkaloids
Ornithine alkaloids
Peptide alkaloids
Pseudoalkaloids
Tetramate alkaloids
Tryptophan alkaloids
Apocarotenoids
Carotenoids (C40)
Diterpenoids
Meroterpenoids
Monoterpenoids
Sesquiterpenoids
Steroids
Triterpenoids
Chromanes
Cyclic polyketides
Linear polyketides
Macrolides
Phloroglucinols
Coumarins
Phenolic acids (C6-C1)
Phenylpropanoids (C6-C3)
Xanthones
Nucleosides
Polyols
Saccharides
Oligopeptides
Small peptides

Black yeasts

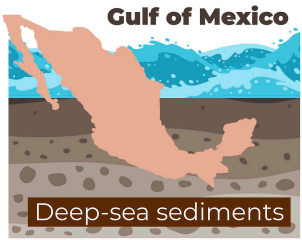

isolation

stress factors

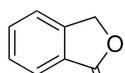

Phthalide (PHT)
Melanin inhibitor

Salinity responses

Morphology and cell division changes

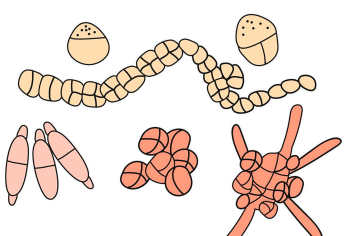

Metabolomic changes